Preparation of AgIn₅S₈/TiO₂ Heterojunction Nanocomposite and Its Enhanced Photocatalytic H₂ Production Property under Visible Light

Kan Li,[†] Bo Chai,*,[†,‡] Tianyou Peng,*,[†] Jing Mao,[†] and Ling Zan[†]

[†]College of Chemistry and Molecular Science, Wuhan University, Wuhan 430072, People's Republic of China
[‡]College of Chemistry and Environmental Engineering, Wuhan Polytechnic University, Wuhan 430023, People's Republic of China

ABSTRACT: AgIn₅S₈/TiO₂ nanocomposite is prepared through a one-pot hydrothermal method, which is used for photocatalytic H₂ production under visible-light irradiation. The effects of AgIn₅S₈/TiO₂ molar ratio in the nanocomposites on the crystal phase, microstructure, optical absorption properties, and photocatalytic H₂ evolution activity are investigated comparatively. The pristine AgIn₅S₈ shows a sharp absorption edge at ~705 nm, corresponding to a bandgap of ~1.76 eV, and its visible-light-driven photoactivity for H₂ production can be remarkably enhanced by coupling with TiO₂. The AgIn₅S₈/TiO₂ nanocomposite with molar ratio of 1:10 has the maximum photoactivity for H₂ production, improved by 7.7 times as compared with the pristine AgIn₅S₈. The enhanced photoactivity can be ascribed to some AgIn₅S₈ nanoparticles closely contacting the TiO₂ nanoparticles to form heterojunction structure. This configuration of the composite photocatalyst results in an efficient charge separation at the interface, followed by fast diffusion of photoelectrons generated in AgIn₅S₈ toward TiO₂, which is beneficial for separating the photogenerated carriers in space and improving the photoactivity.

KEYWORDS: hydrogen production, photocatalyst, AgIn₅S₈, nanocomposite, heterojunction
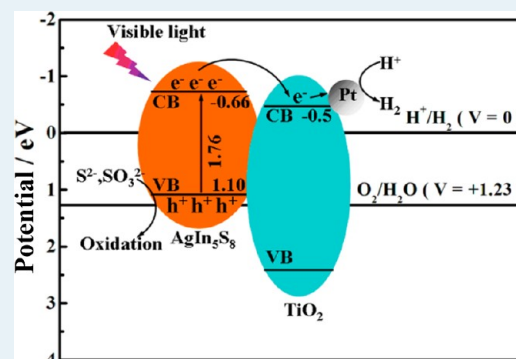
■ INTRODUCTION

Since the photoelectrochemical splitting of water into H₂ and O₂ on TiO₂ a electrode was first reported in 1972,[1] photocatalytic H₂ production over semiconductors has been attracting extensive attention because of its potential applications in the production of clean hydrogen energy.[2] Among these photocatalysts reported, TiO₂ is one of the most promising catalysts because of its easy availability, long-term stability, and nontoxicity.[3] However, the charge recombination usually leads to a low quantum efficiency of TiO₂ as photocatalysts. To resolve this problem, many approaches, such as noble metal loading[3] and coupling with other organic/inorganic materials, have been proposed to enhance the photoactivity of TiO₂.[4−8] As for these coupled TiO₂-based composites, the disadvantages of the individual component can be compensated, resulting in a synergistic effect, such as efficient charge separation and improved photostability. Hence, increasing efforts are focused on coupling TiO₂ with other narrow bandgap semiconductors to form efficient and visible-light-responsive composite photocatalysts.

Semiconductor materials of ternary chalcogenide compounds I−III−VI (I = Cu, Ag; III = Al, In, Ga; VI = S, Se, Te) with a general formula of I−III−VI₂ or I−III₅−VI₈ have been studied in the optoelectronic and photocatalytic fields.[9−17] As one of the ternary chalcogenide compounds, AgIn₅S₈ has direct bandgaps of 1.70−1.80 eV and is considered one of the potential candidates for the visible-light-driven photocatalytic applications. Lee et al.[9] have reported ternary AgIn₅S₈ thin films

deposited on indium tin oxide (ITO)-coated glass substrates using chemical bath deposition (CBD), and the photoresponse experiments indicated that AgIn₅S₈ was suitable for photocatalytic water splitting for visible-light-driven H₂ production. Chen and Ye[15] have also reported that AgIn₅S₈ showed high photoactivity for H₂ evolution under visible-light irradiation. Li et al.[17] have successfully synthesized AgIn₅S₈ nanoparticles by a microwave hydrothermal method and explored its photocatalytic activity for the degradation of methyl orange under visible light. Recently, Kang et al.[18] have reported that a CuInS₂/TiO₂ composite photocatalyst prepared by solvothermal process showed enhanced photoactivity for the degradation of 4-nitrophenol. Jang et al.[19] have reported AgGaS₂/TiO₂ heterojunction photocatalyst fabricated by solid-state reaction and a sol−gel process, and the composites exhibited a greatly improved photoactivity for H₂ production under visible-light irradiation. The above results suggest to us that once AgIn₅S₈ combines with TiO₂, significantly enhanced photoactivity for H₂ production may be realized. To the best of our knowledge, there has been no investigation focused on the AgIn₅S₈/TiO₂ nanocomposite for the photocatalytic H₂ production.

Herein, a series of AgIn₅S₈/TiO₂ nanocomposites were prepared by a one-pot hydrothermal method and used as photocatalyst for the photocatalytic H₂ production under

visible-light ($\lambda \geq 420$ nm) irradiation. It was found that the visible-light-driven photoactivity for H_2 production of $AgIn_5S_8$/TiO_2 nanocomposites were conspicuously enhanced as compared to the pristine $AgIn_5S_8$. Moreover, the effects of the $AgIn_5S_8$/TiO_2 molar ratio in the nanocomposites on the photoactivity for H_2 production were investigated comparatively. The possible mechanism for the enhanced photoactivity was also proposed on the basis of the obtained experimental results.

■ EXPERIMENTAL SECTION

Material Preparation. All chemicals were analytical grade and were used as received without further purification. Commercially available TiO_2 (P25) powder was used as the source of TiO_2. $AgIn_5S_8$/TiO_2 photocatalysts were prepared by a one-pot hydrothermal method. In a typical procedure, a suitable amount of TiO_2, 0.1 mmol of $AgNO_3$, 0.5 mmol of $In(NO_3)_3 \cdot 4.5H_2O$, and 2 mmol of thioacetamide (TAA) were dispersed in 30 mL of distilled water under vigorous stirring. The pH value of the mixed solution was adjusted to 10.2 by using 1.0 M NaOH solution. The mixed solution was then transferred into a 50 mL Teflon-lined autoclave, which was sealed and kept at 180 °C for 24 h and then cooled to room temperature naturally. The precipitate was filtered and washed with distilled water and absolute ethanol several times. The obtained samples were dried in vacuum at 80 °C for 12 h.

For comparison, a series of $AgIn_5S_8$/TiO_2 photocatalysts with different molar ratios (1:2, 1:5, 1:10, and 1:20) were prepared by changing the added amount of TiO_2. Similarly, pristine $AgIn_5S_8$ was also synthesized following the same procedure as mentioned above. Prior to the photocatalytic reaction, Pt cocatalyst was loaded on $AgIn_5S_8$/TiO_2 powders through an in situ photoreduction of H_2PtCl_6 solution under UV-light irradiation of a 500 W high-pressure Hg lamp.[3]

Material Characterization. X-ray powder diffraction (XRD) patterns were obtained using a Bruker D8 Advance X-ray diffractometer with Cu Kα irradiation ($\lambda = 0.154\,178$ nm) at 40 kV and 40 mA. A scan rate of 0.1°/s was applied to record the powder patterns for 2θ in the range of $10° \leq 2\theta \leq 70°$. The morphology of the samples was investigated with field emission scanning electron microscopy using a JSM-6700F microscope. The elemental mapping was characterized by a FEI Nova Nano SEM 630 microscope. The high-resolution transmission electron microscopy (HRTEM) observation was conducted using a LaB$_6$ JEM-2010(HT)-FEF electron microscope working at 140 kV. X-ray photoelectron spectroscopy (XPS) measurement was performed on a Kratos XSAM 800 X-ray photoelectron spectroscope equipped with a standard and monochromatic source (Al Kα) operated at 300 W. The UV−vis diffuse reflectance spectra (DRS) were obtained by a Shimadzu UV-3600 spectrophotometer equipped with an integrating sphere with $BaSO_4$ as the reference sample. The photoluminescence (PL) spectra of samples were measured at room temperature using a fluorescence spectrophotometer (FP-6500, Jasco, Japan) with an excitation wavelength of 315 nm.

Photocatalytic Activity and Photoelectrochemical Measurement. The photocatalytic H_2 production reactions were carried out in an outer irradiation-type photoreactor (Pyrex glass) connected to a closed gas-circulation system. Approximately 0.100 g of Pt-loaded $AgIn_5S_8$/TiO_2 photocatalyst was dispersed by a magnetic stirrer in 100 mL of aqueous solution containing 0.25 M Na_2SO_3 and 0.35 M Na_2S

as sacrificial reagents. Nitrogen was purged through the cell before reaction to remove oxygen. The photocatalysts were irradiated with visible light ($\lambda \geq 420$ nm) using a cutoff filter from a 300 W Xe lamp. The photocatalytic H_2 evolution rate was analyzed with an online gas chromatograph (GC, SP-6890, TCD detector, 5 Å molecular sieve columns and Argon carrier).

Working electrodes were prepared as follows: 0.2 g of sample was ground with 0.8 g of ethanol to make a slurry. The slurry was then coated onto an indium−tin oxide glass by the doctor blade method. These electrodes were dried and calcined at 500 °C for 1 h. All investigated electrodes had a similar film thickness. Photocurrents were measured using an electrochemical analyzer (CHI 618C Instruments) in a standard three-electrode system by using the prepared sample film as the working electrodes (an effective area of 1 cm^2), a Pt flake as the counter electrode, and Ag/AgCl as the reference electrode. Bias potential applied on the working electrode was 0.5 V. A 500 W Xe-lamp (CHF-XM 500, Beijing Trusttech Co. Ltd., China) served as a light source to irradiate the working electrode from the back side. A 1.0 M Na_2SO_4 solution was used as the electrolyte.

■ RESULTS AND DISCUSSION

**Crystal Phase Analyses.** The XRD patterns of $AgIn_5S_8$, TiO_2(P25), and $AgIn_5S_8$/TiO_2 nanocomposites with different molar ratios are shown in Figure 1. As can be seen from Figure
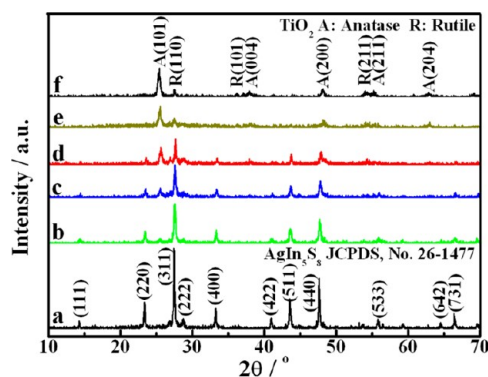
Figure 1. XRD patterns of $AgIn_5S_8$, TiO_2(P25), and $AgIn_5S_8$/TiO_2 nanocomposites with different molar ratios: $AgIn_5S_8$ (a); $AgIn_5S_8$/TiO_2 with molar ratio of 1:2 (b); 1:5 (c); 1:10 (d); 1:20 (e); and TiO_2 (f).

1a, those diffraction peaks at $2\theta = 14.2, 23.2, 27.3, 28.6, 33.2, 40.8, 43.4$, and $47.6°$ can be attributed to the (111), (220), (311), (222), (400), (422), (511), and (440) plane reflections of pure cubic $AgIn_5S_8$ (JCPDS no. 26-1477), respectively. No diffraction peaks other than $AgIn_5S_8$ were detected, indicating that there is no crystal phase impurity existing in the pristine $AgIn_5S_8$, which is in agreement with the literature.[15] The average crystal size of the pristine $AgIn_5S_8$ is ∼34 nm, which is calculated from the prominent and interference-free (400) reflection peak by using Scherrer's equation. After coupling with TiO_2, the XRD patterns consist of $AgIn_5S_8$ and TiO_2 crystal phases, as can be seen in Figure 1b−d. When the $AgIn_5S_8$/TiO_2 molar ratio is changed from 1:2 to 1:20, those diffraction peaks marked with "A" or "R" (Figure 1f), corresponding to the anatase and rutile phase of TiO_2 (P25), are intensified gradually, whereas the peak intensities of $AgIn_5S_8$ decreased. No impurity peak is found in those $AgIn_5S_8$/TiO_2
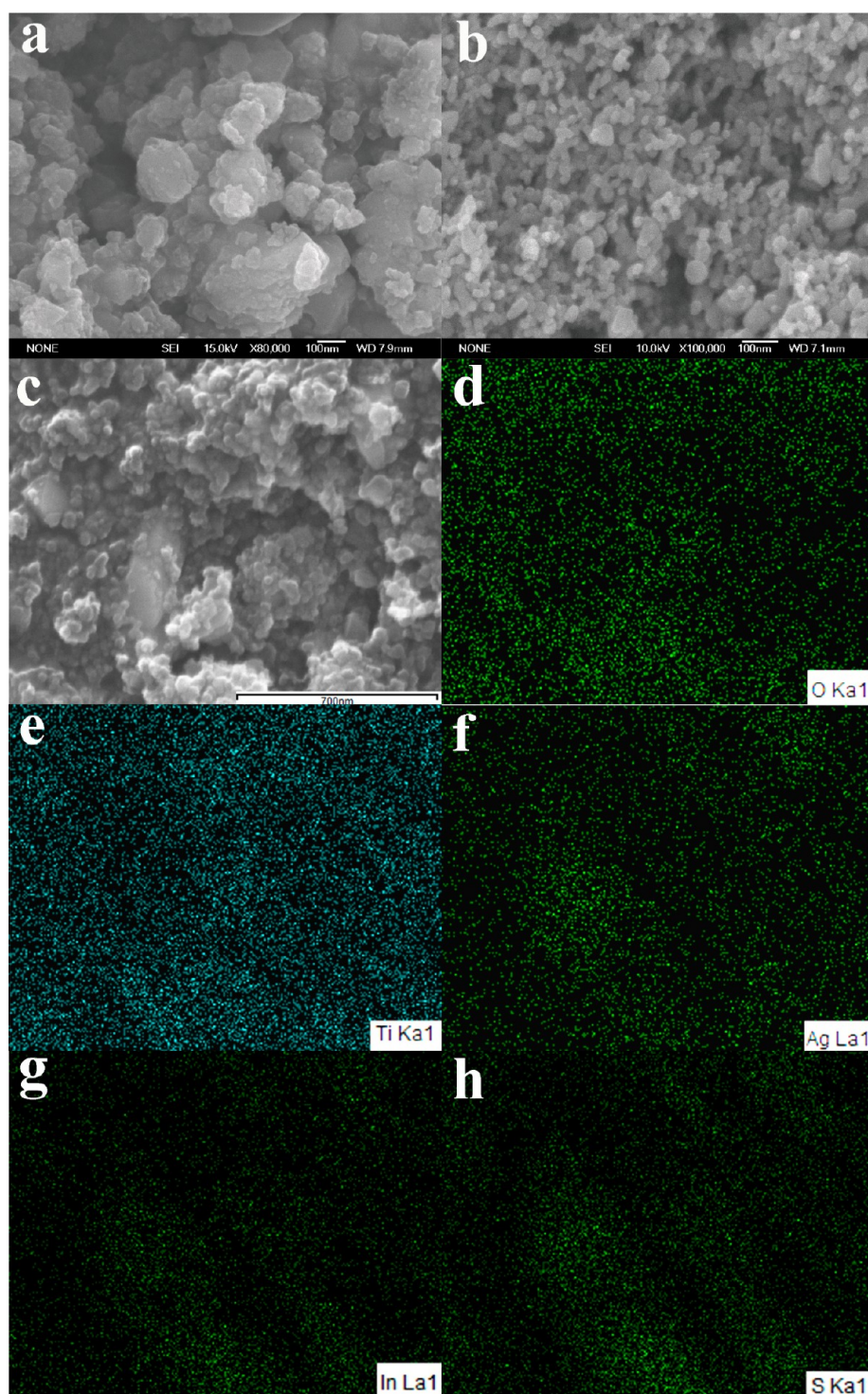
Figure 2. Typical SEM images of $AgIn_5S_8$ (a); TiO_2 (b); and $AgIn_5S_8/TiO_2$ nanocomposite with a molar ratio of 1:10 (c); and the corresponding elemental mapping images for O, Ti, Ag, In, and S of the selected area (c) are presented in d−h.

composites, suggesting that the composites have a two-phase composition: $AgIn_5S_8$ and TiO_2.

The calculated average crystal sizes of $AgIn_5S_8$ in the composites decreased from 32 to 16 nm upon changing the $AgIn_5S_8/TiO_2$ molar ratio from 1:2 to 1:10, implying that the coexisting TiO_2 nanoparticles can retard the crystal growth of the formed $AgIn_5S_8$, which are probably attached to the TiO_2 nanoparticle surfaces; however, the average crystal size calculated from the (101) reflection peak for the pristine

TiO_2 is ∼24 nm, which is similar to those (23−25 nm) of TiO_2 in the $AgIn_5S_8/TiO_2$ nanocomposites with different molar ratios. In addition, no evident shift in the peak positions is observed in those $AgIn_5S_8/TiO_2$ composites. The above results suggest that the TiO_2 crystal lattice was not affected during the present hydrothermal process.

Microstructure Analyses. Typical SEM images of $AgIn_5S_8$, TiO_2(P25), and $AgIn_5S_8/TiO_2$ nanocomposite with a molar ratio of 1:10 are shown in Figure 2. As can been seen, the

pristine $AgIn_5S_8$ shows irregular aggregated nanoparticles with coarse particle surfaces and a broad particle size distribution (Figure 2a), whereas P25 shows much more regular nanoparticles with smooth surfaces and a mean particle size of ~25 nm (Figure 2b). $AgIn_5S_8/TiO_2$ nanocomposite with molar ratio of 1:10 (Figure 2c) also presents obvious agglomeration similar to the pristine $AgIn_5S_8$ but with smaller particle diameters, and many small nanoparticles have a morphology similar to the TiO_2 nanoparticles shown in Figure 2b, which are in close contact with those large aggregated particles with irregular morphology similar to the pristine $AgIn_5S_8$ shown in Figure 2a. The element mappings of O, Ti, Ag, In, and S for the selected area (Figure 2c) measured by the EDS technique are shown in Figure 2d–h. As can be seen, O and Ti signals were very strong, which can be ascribed to the high content of TiO_2 in the composite. All of those signals for O, Ti, Ag, In, and S are very uniform in the observation area, indicating the homogeneous distribution of $AgIn_5S_8$ and TiO_2 in the composite. The above phenomena indicate that the growth of $AgIn_5S_8$ tends to contact the TiO_2 nanoparticles during the present hydrothermal process.

Typical TEM images of $AgIn_5S_8$, TiO_2, and $AgIn_5S_8/TiO_2$ composite with a molar ratio of 1:10 are shown in Figure 3.
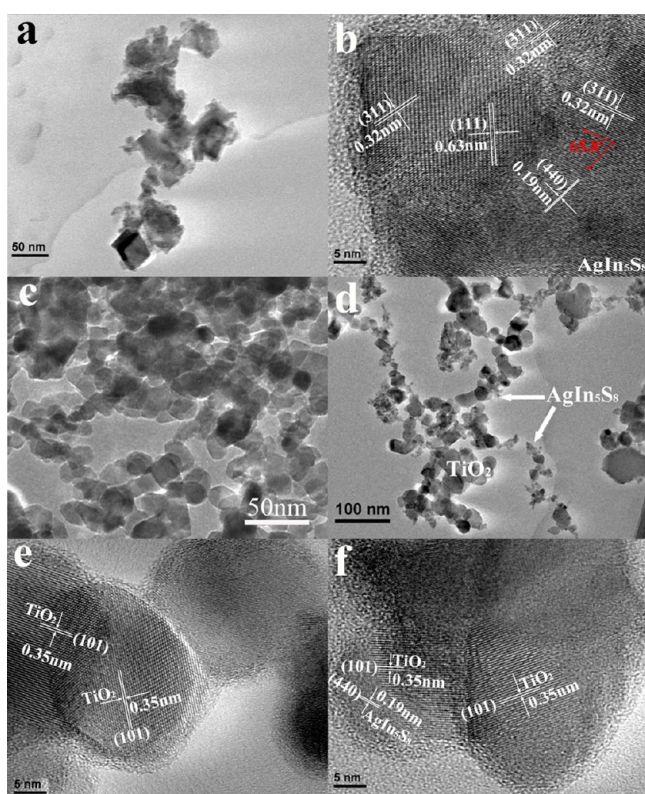
Figure 3. Typical TEM images of $AgIn_5S_8$ (a, b), TiO_2 (c, e), and $AgIn_5S_8/TiO_2$ nanocomposite with a molar ratio of 1:10 (d, f).

The low-magnification TEM image (Figure 3a) shows that the pristine $AgIn_5S_8$ is composed of irregular aggregated particles with coarse surfaces and a broad particle size distribution, which makes it difficult to calculate the average particle diameter. The lattice-resolved HRTEM image (Figure 3b) indicates that the lattice spacing is 0.19, 0.32, and 0.63 nm, which is consistent with the (440), (311), and (111) planes of cubic $AgIn_5S_8$, respectively. Figure 3c shows that P25 has more regular

nanoparticles with smooth surfaces and a mean particle size of 25 nm, which is similar to the above calculated average crystal size and the SEM observation in Figure 2b. A TEM image (Figure 3d) confirms that the $AgIn_5S_8/TiO_2$ nanocomposite with a molar ratio of 1:10 consists of some nanoparticles with smooth surfaces, which is similar to those shown in Figure 3c and can be ascribed to the TiO_2 (P25) nanoparticles, and some other nanoparticles and their aggregations with coarse surfaces and irregular shapes, which is similar to those shown in Figure 3a and therefore can be ascribed to the $AgIn_5S_8$ nanoparticles. Most of those $AgIn_5S_8$ nanoparticles are grown and attached on the TiO_2 particle surfaces.

The above calculated average crystal size (~16 nm) of $AgIn_5S_8$ in the composite with molar ratio of 1:10 is unmatched with the particle diameters of $AgIn_5S_8$ shown in Figure 3d. It might be ascribed to the broad particle size distribution (Figure 3d) of the aggregated $AgIn_5S_8$ derived from the present hydrothermal method; however, the clear lattice fringes in Figure 3e and f indicate the high crystallinity of $AgIn_5S_8$ and TiO_2, which is consistent with the above XRD analyses results. In Figure 3f, the interplanar spacings measured at 0.19 and 0.35 nm, which are similar to those shown in Figure 3b and e, can be assigned to the (440) plane of cubic $AgIn_5S_8$ and the (101) plane of anatase TiO_2, respectively. The above results suggest that some of the formed $AgIn_5S_8$ nanoparticles are in intimate contact with TiO_2 in the nanocomposites. It is obvious that the present synthesis route successfully achieves $AgIn_5S_8/TiO_2$ heterostructure integrating the cubic $AgIn_5S_8$ with the TiO_2 nanoparticles, although part of the $AgIn_5S_8$ particles might just form on their own during the present static hydrothermal process. Further control experiments were conducted to investigate the effects of more (or less) $AgIn_5S_8/TiO_2$ heterostructures on the photoactivity, which will be discussed in the following section.

XPS and UV–vis Absorption Spectra Analyses. XPS was carried out to determine the chemical composition and valence states of various species. Figure 4a displays the XPS survey spectrum for the $AgIn_5S_8/TiO_2$ nanocomposite, which shows Ag 3d, In 3d, S 2p, Ti 2p, O 1s, and C 1s peaks. The regional spectrum of Ag 3d (Figure 4b) presents two peaks with binding energies of 367.6 eV for Ag $3d_{5/2}$ and 373.7 eV for Ag $3d_{3/2}$. The peaks at binding energies of 444.7 and 452.2 eV can be attributed to In $3d_{5/2}$ and In $3d_{3/2}$ (Figure 4c), respectively. In addition, binding energy peaks at 459.1 and 464.8 eV are in agreement with the Ti $2p_{3/2}$ and Ti $2p_{1/2}$ (Figure 4e), respectively. The binding energy values are very close to the reported ones, indicating that the valence states of Ag, In, and Ti are +1, +3, and +4, respectively,[17,20] although the spectrum of S 2p (Figure 4d) shows a broad asymmetric curve that can be deconvoluted into two peaks with binding energies at 161.3 eV for S $2p_{3/2}$ and 162.5 eV for S $2p_{1/2}$, respectively. The O 1s XPS spectrum is illustrated in Figure 4f, which can be deconvoluted as two peaks. The peaks at 531.8 and 530.3 eV are ascribed to O 1s of H_2O and TiO_2, respectively. These results indicate that the S and O are present as S^{2-} and O^{2-} in the present product, respectively.[17,20]

Figure 5 shows the UV–vis diffuse reflectance spectra of $AgIn_5S_8$, TiO_2(P25) and $AgIn_5S_8/TiO_2$ nanocomposites. As can be seen, TiO_2 presents a steep absorption edge at ~410 nm, which can be assigned to the intrinsic bandgap absorption of TiO_2. As for $AgIn_5S_8$, the spectrum shows a sharp absorption edge at ~705 nm, which is in good agreement with the reported result.[15] The bandgap of $AgIn_5S_8$ is estimated to be

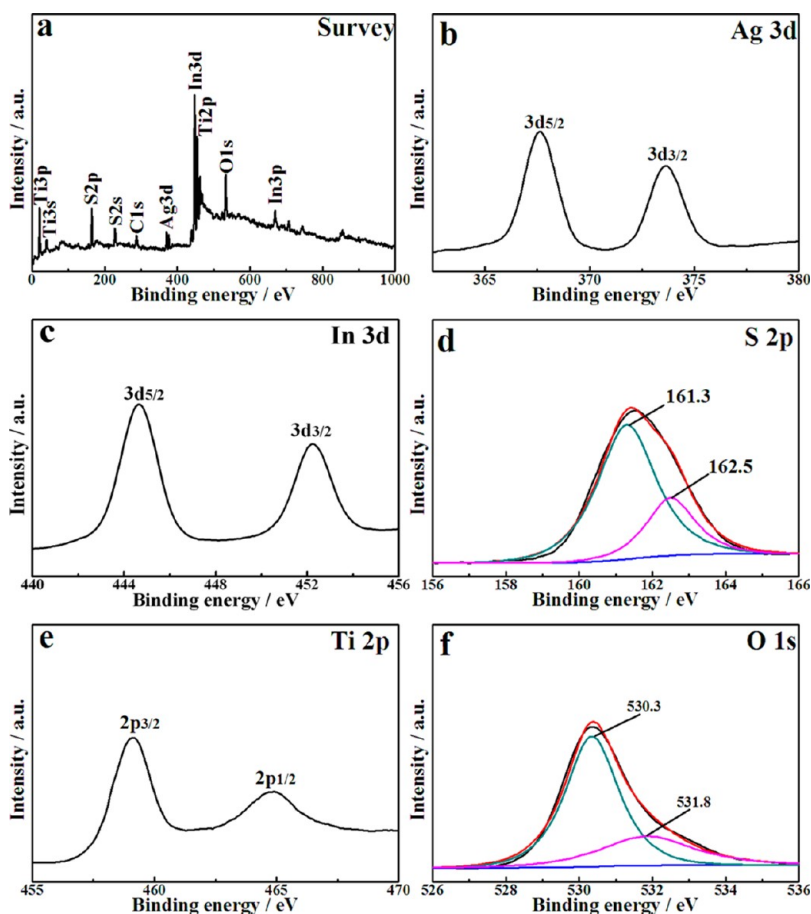**Figure 4.** XPS spectra of $AgIn_5S_8/TiO_2$ nanocomposite with a molar ratio of 1:10.

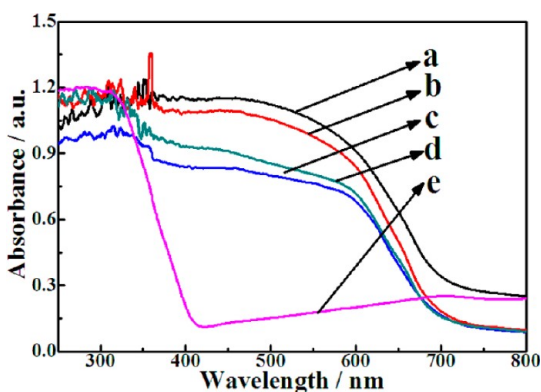**Figure 5.** UV−vis diffuse reflectance spectra of TiO_2(P25), $AgIn_5S_8$ (a) and $AgIn_5S_8/TiO_2$ with molar ratio of 1:5 (b); 1:10 (c); 1:20 (d); and TiO_2 (e).

1.76 eV according to the equation of $E_g = 1240/\lambda_g$, where λ_g is the optical absorption edge of semiconductor. The absorption spectra of $AgIn_5S_8/TiO_2$ nanocomposites show the combination of these two DRS spectra contributing from TiO_2 and $AgIn_5S_8$, and the characteristic absorption peak slightly blue-shifts with decreasing intensities compared wiht the pristine $AgIn_5S_8$ when the $AgIn_5S_8/TiO_2$ molar ratio is changed from 1:5 to 1:20. As a result, those $AgIn_5S_8/TiO_2$ nanocomposites exhibit a wide spectral response performance.

Photocatalytic H_2 Evolution Activity and Stability. Control experiments showed no appreciable H_2 evolution without light irradiation or photocatalyst in the photocatalytic

reaction system. To improve the photoactivity of H_2 production, 2.0 wt % Pt as cocatalyst was loaded on the photocatalysts to provide active sites. Photocatalytic H_2 production rates over $AgIn_5S_8$, TiO_2(P25), and $AgIn_5S_8/TiO_2$ nanocomposites with different molar ratios under visible-light irradiation ($\lambda \geq 420$ nm) are shown in Figure 6. As can be seen, the H_2 production rate of Pt-loaded $AgIn_5S_8$ is 11 μmol h^{-1}, whereas Pt-loaded TiO_2 has no obvious H_2 evolution under visible-light irradiation. $AgIn_5S_8/TiO_2$ nanocomposites exhibit remarkable enhancement in the photoactivity for H_2 production. With the $AgIn_5S_8/TiO_2$ molar ratio changing
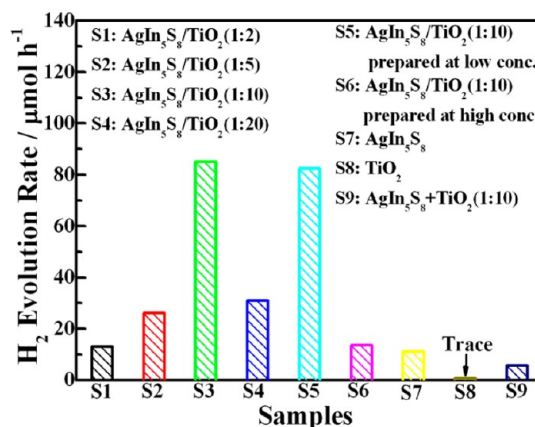

Figure 6. Effect of $AgIn_5S_8/TiO_2$ molar ratio in the nanocomposite on the photocatalytic H_2 evolution rates under visible-light irradiation.

from 1:2 to 1:10, the H_2 production rates greatly increase, and the $AgIn_5S_8/TiO_2$ with a molar ratio of 1:10 shows a maximum photoactivity ($85\ \mu mol\ h^{-1}$) for H_2 production, improved by 7.7 times as compared with the pristine $AgIn_5S_8$, whereas too high a TiO_2-loading level in the composite, such as in the case of $AgIn_5S_8/TiO_2$ with a molar ratio of 1:20, decreased the photoactivity. Nevertheless, all of the $AgIn_5S_8/TiO_2$ composites showed better photoactivity than the pristine $AgIn_5S_8$. In addition, the photoactivity is improved upon the $AgIn_5S_8/TiO_2$ molar ratio changing from 1:2 to 1:10. The above phenomena seem to imply that the enhanced photoactivity probably results from the presence of a $AgIn_5S_8/TiO_2$ interface, and the photoinduced carriers' separation may be dependent on the structure characteristics of $AgIn_5S_8/TiO_2$ because the coexisting TiO_2 nanoparticle amount affects not only the particle growth and morphology but also the $AgIn_5S_8/TiO_2$ interfacial structure, as mentioned above.

To further verify the above assumption on the effects of the interfaces and the structure characteristics of $AgIn_5S_8/TiO_2$, three photocatalysts with the same molar ratio (1:10) were prepared by considering that the $AgIn_5S_8$ particles might just form on their own but not on the coexisting TiO_2 particles during the present static hydrothermal process. One is the physical mixture ($AgIn_5S_8 + TiO_2$), the others are prepared by changing the reactants' concentrations to 0.2 or 5 times the values described in the Experimental section. Usually, the low concentrations of $AgNO_3$, $In(NO_3)_3$, and TAA are beneficial for growth of $AgIn_5S_8$ on the coexisting TiO_2 nanoparticle surfaces to form intimate contacts, whereas the high reactant concentrations can enhance the probability of $AgIn_5S_8$ just formed on its own, resulting in less components' contacts, and there is much less intimate contact between the components in the physical mixture.

The above three photocatalysts were used for H_2 production under the same photoreaction conditions. As can be seen from Figure 6, the physical mixture shows only a very low photocatalytic H_2 production activity ($5.6\ \mu mol\ h^{-1}$), and the $AgIn_5S_8/TiO_2$ derived from the high concentration has a low photoactivity ($13.6\ \mu mol\ h^{-1}$), whereas the $AgIn_5S_8/TiO_2$ derived from the low concentration shows a higher photo-activity ($82.2\ \mu mol\ h^{-1}$), which is similar to that ($85\ \mu mol\ h^{-1}$) of the as-prepared $AgIn_5S_8/TiO_2$. The above results indicate that the intimate contact between $AgIn_5S_8$ and TiO_2 is crucial for enhancing the photoactivity, and the present hydrothermal conditions lead to some $AgIn_5S_8$ nanoparticles coming in close contact with TiO_2 particles to form a heterostructure, although it is inevitable that some other $AgIn_5S_8$ separated from the TiO_2 nanoparticles in the present static hydrothermal condition, even in the low reactant concentrations.

Figure 7 depicts the photostability of $AgIn_5S_8/TiO_2$ nanocomposites, which are investigated in three consecutive runs of accumulatively 15 h with fresh sacrificial reagents solution periodically replaced in each run. No noticeable decrease in the photoactivity was found for the present composite photocatalysts when the reaction time was extended. This fairly good stability of the present composite photocatalyst can be ascribed to the existence of SO_3^{2-}/S^{2-} as sacrificial reagents. The photogenerated electrons in the conduction band (CB) of $AgIn_5S_8$ can transfer to TiO_2 and reduce the water to form H_2. Meanwhile, the SO_3^{2-} and S^{2-} change into SO_4^{2-} and S_2^{2-} by the photogenerated holes in the valence band (VB) of $AgIn_5S_8$, and the production of S_2^{2-} is efficiently suppressed by reaction with SO_3^{2-}. Moreover, the presence of excessive S^{2-} in
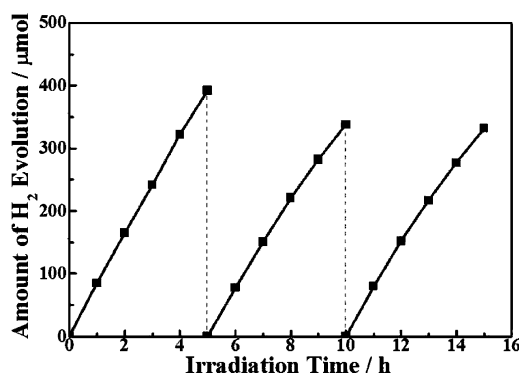
Figure 7. Stability study of photocatalytic H_2 evolution over $AgIn_5S_8/TiO_2$ nanocomposite with a molar ratio of 1:10 under visible-light irradiation.

the reaction solution can also suppress the formation of sulfur defects and stabilizes the photocatalyst. The XRD pattern (Figure 8) of the recycled $AgIn_5S_8/TiO_2$ after 15 h of
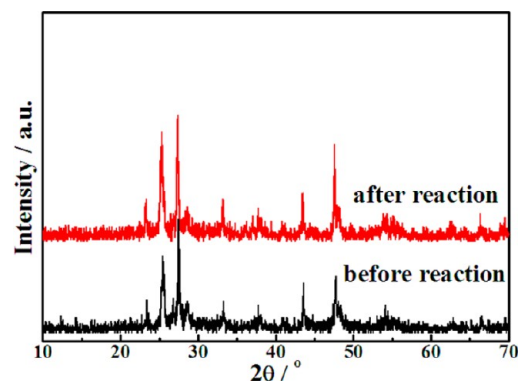
Figure 8. XRD patterns of $AgIn_5S_8/TiO_2$ with a molar ratio of 1:10 before and after 15 h of photocatalytic H_2 evolution reaction.

photoreaction is essentially similar to that of the original one, and there is no obvious deviation in the locations of these peaks, indicating that $AgIn_5S_8/TiO_2$ nanocomposite has considerable photostability.

Discussion on the Mechanism of the Enhanced Photoactivity. On the basis of the above experimental results and discussion, a proposed mechanism for the enhanced photoactivity over the present $AgIn_5S_8/TiO_2$ is shown schematically in Figure 9. Under visible-light illumination, the
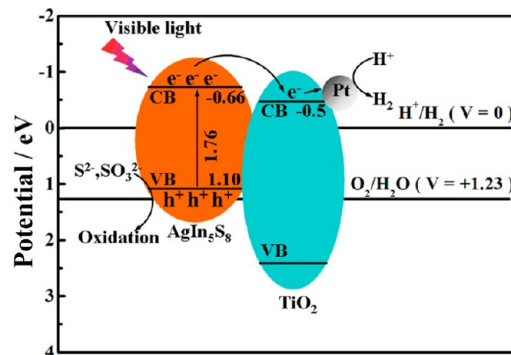
Figure 9. The proposed photocatalytic H_2 evolution mechanism over $AgIn_5S_8/TiO_2$ nanocomposite under visible-light irradiation.

photogenerated electrons are excited from the VB to the CB of $AgIn_5S_8$, creating positive holes in the VB of $AgIn_5S_8$. As a result, the sacrificial reagents are oxidized by the positive holes in the VB of $AgIn_5S_8$, and the photoexcited electrons in the CB of $AgIn_5S_8$ can migrate and inject to TiO_2, following transfer to the loaded Pt nanoparticles to generate H_2. Hence, the remarkably increased photoactivity for the present $AgIn_5S_8/TiO_2$ can be ascribed to the efficient separation of the photogenerated electron−hole pairs in the present system. The better photogenerated carrier separation efficiency in $AgIn_5S_8/TiO_2$ is confirmed by the photoluminescence spectra (Figure 10). The PL spectrum for TiO_2 is characterized by two
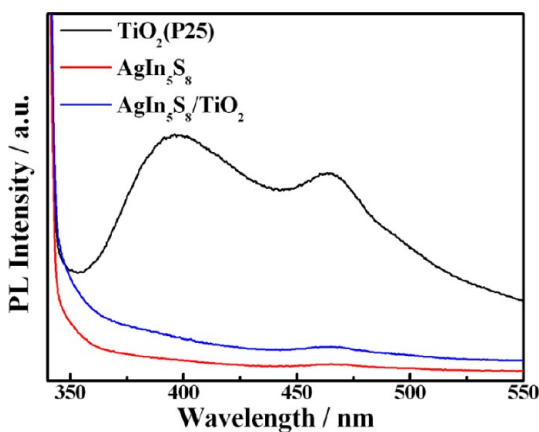

Figure 10. PL spectra of $AgIn_5S_8$, TiO_2, and $AgIn_5S_8/TiO_2$ nanocomposite with a molar ratio of 1:10.

main peaks around 392 and 464 nm, which are attributed to the emission of bandgap transition and surface oxygen vacancies and defects, respectively. It is found that $AgIn_5S_8/TiO_2$ with a molar ratio of 1:10 exhibits a fluorescence decrease (or quenching) as compared with TiO_2, indicating that the photogenerated carrier recombination is inhibited greatly. These results should be derived from the imitate contacts between $AgIn_5S_8$ and TiO_2.

For further verification of the above proposed mechanism, the band edge potentials of semiconductors were estimated using the equation related to Mulliken electronegativity. Herein, the electronegativity of an atom is the arithmetic mean of the atomic electron affinity and the first ionization energy, and the CB and VB potential can be calculated according to an empirical equation:[7]

$$E_{CB} = X − E^e − 0.5E_g \quad (1)$$

$$E_{VB} = E_{CB} + E_g \quad (2)$$

where E_{CB} is the CB edge potential, X is the electronegativity of the semiconductor, which is the geometric mean of the electronegativity of the constituent atoms, E^e is the energy of free electrons on the hydrogen scale (~4.5 eV), and E_g is the bandgap energy of the semiconductor.

The CB and VB potentials of $AgIn_5S_8$ have been calculated to be $E_{CB} = −0.66$ eV and $E_{VB} = 1.10$ eV, which is in good agreement with the reported results.[12] The CB position of TiO_2 (P25) was determined via the electrochemical method by Fu et al., indicating that the CB position was −0.5 eV (NHE).[21] As a result, the CB edge potential of $AgIn_5S_8$ is more negative than that of TiO_2. On one hand, the increase in photoactivity at changing the $AgIn_5S_8/TiO_2$ molar ratio from 1:2 to 1:10 (with

TiO_2 content increase) may be ascribed to the synergistic effect between the $AgIn_5S_8$ and TiO_2. The CB electrons of $AgIn_5S_8$ easily flow into the CB edge of TiO_2 via the interface; namely, the TiO_2 can act as a sink of photogenerated electrons of $AgIn_5S_8$, and the enhanced TiO_2 amount is beneficial for promoting the carriers separated in space and hindering the charge recombination. The higher photogenerated carrier separation probability would lead to reduced carrier recombination and enhanced photoactivity of the composite photocatalyst. On the other hand, the decrease in photoactivity at higher TiO_2-loading levels may result from the excessive TiO_2 shielding $AgIn_5S_8$ from the incident light and hindering contact with the sacrificial reagents responsible for the hole reaction. Another possible reason may be ascribed to the relative amount decrease of the active $AgIn_5S_8$ because the same amount (100 mg) of photocatalyst was used for the above photoreaction.

The higher carrier separation probability of $AgIn_5S_8/TiO_2$ nanocomposite can also be observed from the photocurrent responses ($I−t$ curve) of the photoelectrodes consisting of $AgIn_5S_8$, TiO_2, and the $AgIn_5S_8/TiO_2$ nanocomposite with a molar ratio of 1:10 (Figure 11). As can be seen, the stable
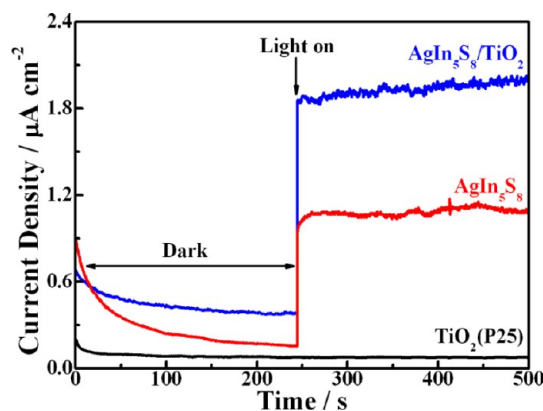

Figure 11. The photocurrent responses of the film electrodes made of $AgIn_5S_8$, TiO_2, and $AgIn_5S_8/TiO_2$ nanocomposite with a molar ratio of 1:10 in 1.0 M Na_2SO_4 solution under visible-light irradiation.

photocurrent value of $AgIn_5S_8/TiO_2$ is ~1.8 times as high as that of the pristine $AgIn_5S_8$, which can be ascribed to the close interfacial connections and the synergetic effect existing in the $AgIn_5S_8/TiO_2$ interface, where photogenerated electrons and holes are efficiently separated in space, and resulting in reduced photoinduced carrier recombination, corresponding to its enhanced photocurrent. Therefore, it can be concluded that the proposed fabrication of the heterojunction system consisting of $AgIn_5S_8$ and TiO_2 nanoparticles can be a successful and generic strategy to develop highly active photocatalysts under visible light.

■ CONCLUSION

In summary, wide spectral responsive $AgIn_5S_8/TiO_2$ heterojunction nanocomposites are successfully prepared by a one-pot hydrothermal method. The investigation of their photocatalytic ability shows that the $AgIn_5S_8/TiO_2$ composite possess a higher photoactivity for H_2 production than the pristine $AgIn_5S_8$ under visible-light ($\lambda \geq 420$ nm) irradiation. SEM and TEM reveal that some $AgIn_5S_8$ nanoparticles are grown and closely attached on the TiO_2 nanoparticles surfaces, and the phase structure and crystallite size of TiO_2 in the composites have no significant

change as compared with the added TiO_2 during the hydrothermal process. This combination is beneficial for the formation of the heterojunction, which can result in a synergistic effect of various components and significant enhancement of the photogenerated carrier separation and then the improvement of the photocatalytic H_2 production activity. The optimal molar ratio of $AgIn_5S_8/TiO_2$ is found to be 1:10, and the corresponding H_2 production rate is 85 μmol h^{-1}, which exceeds that of the pristine $AgIn_5S_8$ by 7.7 times. Therefore, the present experimental procedure for the novel $AgIn_5S_8/TiO_2$ heterostructure is quite simple, environmentally benign, and cost-effective, permitting it to be applied in the synthesis of future heterostructured photocatalysts.

■ AUTHOR INFORMATION

Corresponding Author
*Phone, fax: +86-27 6875 2237. E-mails: typeng@whu.edu.cn (T.P.), willycb@163.com (B.C.).

Author Contributions
The manuscript was written through contributions of all authors. All authors have given approval to the final version of the manuscript.

Notes
The authors declare no competing financial interest.

■ ACKNOWLEDGMENTS

■ REFERENCES

(1) Fujishima, A.; Honda, K. *Nature* **1972**, *238*, 37−38.

(2) Chen, X. B.; Shen, S. H.; Guo, L. J.; Mao, S. S. *Chem. Rev.* **2010**, *110*, 6503−6570.

(3) Yi, H. B.; Peng, T. Y.; Ke, D. N.; Dai, K.; Zan, L.; Yan, C. H. *Int. J. Hydrogen Energy* **2008**, *33*, 672−678.

(4) Lin, Y. M.; Li, D. Z.; Hu, J. H.; Xiao, G. C.; Wang, J. X.; Li, W. J.; Fu, X. Z. *J. Phys. Chem. C* **2012**, *116*, 5764−5772.

(5) Yan, H. J.; Yang, H. X. *J. Alloys Compd.* **2011**, *509*, L26−L29.

(6) Qian, S. S.; Wang, C. S.; Liu, W. J.; Zhu, Y. H.; Yao, W. J.; Lu, X. H. *J. Mater. Chem.* **2011**, *21*, 4945−4952.

(7) Chai, B.; Peng, T. Y.; Zeng, P.; Mao, J. *J. Mater. Chem.* **2011**, *21*, 14587−14593.

(8) Shang, M.; Wang, W. Z.; Zhang, L.; Sun, S. M.; Wang, L.; Zhou, L. *J. Phys. Chem. C* **2009**, *113*, 14727−14731.

(9) Chang, W. S.; Wu, C. C.; Jeng, M. S.; Cheng, K. W.; Huang, C. M.; Lee, T. C. *Mater. Chem. Phys.* **2010**, *120*, 307−312.

(10) Qasrawi, A. F. *J. Alloys Compd.* **2008**, *455*, 295−297.

(11) Lin, L. H.; Wu, C. C.; Lai, C. H.; Lee, T. C. *Chem. Mater.* **2008**, *20*, 4475−4483.

(12) Cheng, K. W.; Wang, S. C. *Mater. Chem. Phys.* **2009**, *115*, 14−20.

(13) Wang, D. S.; Zheng, W.; Hao, C. H.; Peng, Q.; Li, Y. D. *Chem. Commum.* **2008**, 2556−2558.

(14) Lin, L. H.; Wu, C. C.; Lee., T. C. *Cryst. Growth Des.* **2007**, *12*, 2727−2732.

(15) Chen, D.; Ye, J. H. *J. Phys. Chem. Solids* **2007**, *68*, 2317−2320.

(16) Zhang, W. J.; Li, D. Z.; Chen, Z. X.; Sun, M.; Li, W. J.; Lin, Q.; Fu, X. Z. *Mater. Res. Bull.* **2011**, *46*, 975−982.

(17) Zhang, W. J.; Li, D. Z.; Sun, M.; Shao, Y.; Chen, Z. X.; Xiao, G. C.; Fu, X. Z. *J. Solid State Chem.* **2010**, *183*, 2466−2474.

(18) Kang, S. Z.; Yang, Y. K.; Bu, W. B.; Mu, J. *J. Solid State Chem.* **2009**, *182*, 2972−2976.

(19) Jang, J. S.; Hong, S. J.; Kim, J. Y.; Lee, J. S. *Chem. Phys. Lett.* **2009**, *475*, 78−81.

(20) An, G. M.; Ma, W. H.; Sun, Z. Y.; Liu, Z. M.; Han, B. X.; Miao, S. D.; Miao, Z. J.; Ding., K. L. *Carbon* **2007**, *45*, 1795−1801.

(21) Huang, H. J.; Li, D. Z.; Lin, Q.; Zhang, W. J.; Shao, Y.; Chen, Y. B.; Sun, M.; Fu, X. Z. *Environ. Sci. Technol.* **2009**, *43*, 4164−4168.